APPLIED GEOPHYSICS, Vol.18, No.3 (September 2021), P. 277–287, 7 Figures.
DOI:10.1007/s11770-021-0899-x

# Forward modeling of tight sandstone permeability based on mud intrusion depth and its application in the south of the Ordos Basin*

Liu Wen-hui[1], Lv Xiao-Chun♦[1], and Shen Bo[2]

**Abstract**: Permeability is an important index in reservoir evaluation, oil and gas accumulation control, and production efficiency. At present, permeability can be obtained through several methods. However, these methods are not suitable for tight sandstone in general because the pore type in tight sandstone is mainly secondary pores and has the characteristics of low porosity and permeability, high capillary pressure, and high irreducible water saturation. Mud invasion depth is closely related to permeability during drilling. In general, the greater the permeability, the shallower the mud invasion depth, and the smaller the permeability, the deeper the mud invasion depth. Therefore, this paper builds a model to predict the permeability of tight sandstone using mud invasion depth. The model is based on the improvement of the Darcy flow equation to obtain permeability using mud invasion depth inversion of array induction logging. The influence of various permeability factors on the model is analyzed by numerical simulation. The model is used to predict the permeability of tight sandstone in the south of the Ordos Basin. The predicted permeability is highly consistent with the core analysis permeability, which verifies the reliability of the method.
**Keywords**: permeability evaluation, Darcy flow equation, numerical simulation, mud invasion depth, array induction logging

## Introduction

Permeability is a parameter that represents the difficulty of fluid flow in rocks. It has an important influence on reservoir evaluation, reservoir model establishment, reservoir simulation, productivity prediction, recovery factor improvement, and exploration and development plan making for tight sandstone (Orlov et al., 2021; Chen et al., 2017; Timur, 1969). Therefore, accurate permeability prediction is of great significance for the exploration and development of tight sandstone. However, high-accuracy permeability calculation is considered very difficult. The range of methods used to estimate permeability can be classified into three distinct general categories: experimental, statistical, and mathematical methods (Lala, 2019). At present, experimental methods are the most accurate

Manuscript received by the Editor January 4, 2020; revised manuscript received December 21, 2020.
*This work was supported by the National Natural Science Foundation of China project (No. 41504103 and No. 41804097).
1. North China University of Water Resources and Electric Power, College of Geosciences and Engineering, Zhengzhou 450045, China.
2. Yangtze University, Geophysics and Oil Resource Institute, Wuhan 430010, China.
♦Corresponding author: Lv Xiao-Chun (Email: xc66995618@163.com).

methods to determine permeability, including measuring the permeability, porosity, and water saturation of cylindrical rock samples, then constructing mathematical equations with high coefficients of transgression that show the relationship between porosity and irreducible water saturation with permeability (Alfi et al., 2019). For example, the Kozeny–Carman equation permeability model, based on an empirical formula, fits well in predicting the permeability of conventional sandstone (Pape et al., 1999; Costa, 2006). However, this model is not suitable for a tight sandstone reservoir because of its complexity in terms of pore structure and type. In addition, this model has obvious defects in timeliness and economy due to the need for a large number of laboratory core data. To solve this problem, scholars at home and abroad have carried out a lot of research and established a variety of permeability prediction models using statistical methods for tight sandstone reservoirs. These prediction models are established mainly based on mercury injection test data and various logging data. For example, Tong et al. (2008) established a permeability model using a combination of capillary pressure curves and Darcy flow equation. However, this method is greatly affected by the permeability variation range. To improve accuracy, it is necessary to establish parameter prediction models in different microphases. Al-Marzouqi (2018) built a digital core model based on CT scanning of cylindrical cores and laboratory analysis data and simulated fluid flow characteristics in porous media. However, it is not effective for rocks with cracks. Mao et al. (2013) combined nuclear magnetic resonance (NMR) logging and mercury injection data to establish a permeability calculation method by analyzing the relationship between Swanson parameters and permeability. However, the relationship between the T2 cutoff value of NMR and the mercury injection capillary pressure (Swanson parameter) is established by a fitting method, and its accuracy is greatly affected by the number of sample points. Paulina and Edyta (2015) predicted permeability using NMR, mercury porosimetry, and computer microtomography laboratory techniques. Selection of the T2 cutoff value of NMR is difficult in this method. Fan et al. (2018) subdivided the pore space based on the double cutoff value of NMR and established a new permeability model based on analysis of the influence of different pore components on permeability. However, a limitation of this method is that there are great differences in the morphology of nuclear magnetic spectrum peaks in gas or heavy oil layers, which leads to low precision of double cutoff values and affects the accuracy of permeability calculation. Based on lithologic composition analysis, Uspenskaya et al. (2012) used the stoneley wave to predict permeability, but the effect on tight sandstone still needs to be further verified. Based on Lambda model, Li et al. (2015) evaluated the permeability of tight sandstone reservoirs by using mineral composition and skeleton density obtained from elemental capture spectroscopy (ECS) logging. However, because of the lack of ECS logging data, it is difficult to obtain permeability calculation models for large areas. In addition, with the rapid development of computer technology, some mathematical methods have been applied to permeability calculations: Larson et al. (1981) introduced percolation theory to permeability evaluation, Zhang et al. (2019) combined a capillary bundle model and fractal theory and established a mathematical model of pore-scale parameters and hydrocarbon migration process in low-permeability formations, Saemi et al. (2007) and Al-Anazi and Gates (2012) used neural network theory to train several logging parameters and matched permeability according to the training results, and Abdulraheem et al. (2007) used the fuzzy logic algorithm for well logging-based permeability modeling. Mahdaviara et al. (2020) adopted a new permeability calculation method, namely least squares support vector machine modeling optimized with a coupled simulated annealing optimization technique. Then, statistical and graphical error analyses were employed separately to evaluate the accuracy and reliability of the proposed model. These methods have their own advantages, but for tight sandstone reservoirs with complex occurrence mechanisms and unclear seepage law, they need further improvement of accuracy.

Permeability is an important factor affecting mud invasion depth, so mud invasion depth can be used to predict permeability. It is difficult to directly obtain permeability; however, mud invasion depth can be obtained by logging data inversion. Array induction logging can obtain six resistivity curves, and the radial detection range can cover the resistivity of the flushed zone, the intrusion zone, and the undisturbed formation. Mud invasion depth can be quickly and accurately inverted using array induction logging data ( Pardo et al., 2015; Feng et al., 2015). In this paper, a permeability model based on mud invasion depth was established by using the inversion of array induction

logging of tight sandstone reservoirs and the improved Darcy flow equation. The accuracy of the model has been verified by actual data.

## Establishment of the permeability calculation model

Darcy's flow law describes the relationship between fluid flux and pressure gradient (Darcy, 1856) and is the most basic law to predict permeability (He et al., 2007). According to the law, the invasion rate of a mud filtrate is given by

$$v = -\frac{k}{\mu_w} g \frac{\partial P}{\partial r}, \tag{1}$$

where $k$ is the formation permeability (mD), $\mu_w$ is the water viscosity (Pa·s), $P$ is the fluid pressure (Pa), and $r$ is the radial distance from the borehole axis (m).

Then, the flow per unit time through the cylinder side area with a radius of $r$ is given by

$$q = vA = -\frac{2\pi rhk}{\mu_w} \frac{\partial P}{\partial r}, \tag{2}$$

where $A$ is the cylinder side area ($m^2$) and $h$ is the formation thickness (m).

Equation (2) is changed into

$$q\frac{\partial r}{r} = -\frac{2\pi hk}{\mu_w}\partial P. \tag{3}$$

Integrating both sides of equation (3) gives

$$\int_{r_w}^{r_e} q \frac{dr}{r} = -\int_{P_w}^{P_e} \frac{2\pi hk}{\mu_w} dP, \tag{4}$$

where $r_w$ is the borehole diameter (m), $r_e$ is the distance of the preset boundary to the borehole axis (m), $P_w$ is the borehole pressure (Pa), and $P_e$ is the reservoir boundary pressure (Pa).

Equation (4) is simplified and rearranged to obtain the flow rate of the mud filtrate into the reservoir per unit time as

$$q = \frac{2\pi hk}{\mu_w} \frac{(P_w - P_e)}{\ln\left(\frac{r_e}{r_w}\right)}. \tag{5}$$

Then, the total fluid flow from the wellbore to the reservoir in a specified time $T'$ is

$$Q = qT' = \frac{2\pi hkT'}{\mu_w} \frac{(P_w - P_e)}{\ln\left(\frac{r_e}{r_w}\right)}. \tag{6}$$

The inversion problem of array induction logging is the optimization selection of multiple parameters. Three- and five-parameter inversion models are the most commonly used models. However, three-parameter inversion is limited by the idealized step intrusion model and finite measured data, which greatly affects the accuracy of inversion. The five-parameter inversion model is a more complex gradient model, which divides the invaded zone into two parts: the flushed zone and the transitional zone, which is closer to the actual formation. The damped least-squares method and the optimized variable scale method are used to carry out the inversion; then, five parameters can be obtained: the resistivities of the flushed zone, the transitional zone, and the undisturbed formation and the radius of the flushed and invaded zones (Li et al., 2012). This model improves the multisolution of the inversion, constrains the distribution range of the solution, and improves the reliability of the inversion problem. In this inversion model, it is assumed that the invasion is step-type, i.e., the invasion is a simple ring form without considering the influence of the gradual transitional zone. Then, according to the invasion depth, the total fluid flow in the formation pores of the invaded zone can be obtained by

$$Q = \left(\pi L^2 - \pi r_w^2\right)h\phi(1 - S_{or}), \tag{7}$$

where $L$ is the radius of the mud invasion leading edge to the borehole axis (m), $\varphi$ is the formation porosity, and $S_{or}$ is the remaining oil saturation.

Equations (6) and (7) are combined to get

$$k = \frac{\left(L^2 - r_w^2\right)\phi(1 - S_{or})\mu_w \ln\left(\frac{r_e}{r_w}\right)}{2T'(P_w - P_e)}. \tag{8}$$

Equation (8) establishes the permeability calculation model for tight sandstone. The model shows that permeability can be calculated using invasion depth and other measurable parameters (mud invasion depth can be obtained by inversion of array induction logging

with five parameters, and the other parameters can be obtained using logging and formation test data).

The mud invasion model used in the permeability model is shown in Figure 1.

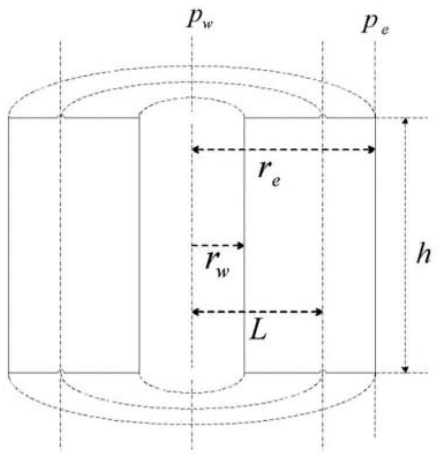


**Figure 1. Geometric model used in the permeability calculation.**

It should be noted that $r_e$ should be much greater than $r_w$ in the calculation. Therefore, it is necessary to keep $r_e$ large enough to make it possible for the outer boundary of the mud invasion process not to be affected by wellbore pressure, and then the outer boundary pressure can be equal to the initial pressure of the reservoir. In the numerical simulation, a constant-pressure boundary is adopted for the outer boundary, i.e., it is assumed that the outer boundary is not affected by wellbore pressure, so the calculated results are not affected. However, once this method is combined with the actual production, the influence of the outer boundary must be taken into account. Therefore, it is necessary to keep the outer boundary as far away from the wellbore as possible so that the initial reservoir pressure obtained by logging can be used as the outer boundary pressure in the mathematical model.

In addition, due to borehole mud cake fracture or borehole collapse, well leakage, necking, differential pressure sticking, and other engineering factors caused by poor well conditions, mud invasion will be seriously affected, resulting in insufficient accuracy of permeability inversion (Liu et al., 2012; Feng, 2019). Therefore, when using this model, it is best to select intervals with regular borehole diameter for inversion calculation.

# Analysis of influencing factors of permeability

## Invasion depth

To test the reliability of the model, it is first verified in a one-dimensional mud invasion model, and the basic parameters are shown in Table 1.

**Table 1 Basic parameters of the one-dimensional mud invasion model**

| Parameter name | Parameter value | Parameter name | Parameter value |
|---|---|---|---|
| initial porosity | 0.2 | mud salinity (ppm) | 10000 |
| original formation permeability (mD) | 1 | formation water salinity (ppm) | 100000 |
| initial density of water (g/cm$^3$) | 1.05 | well radius (m) | 0.1016 |
| initial density of oil (g/cm$^3$) | 0.95 | reservoir radius (m) | 9.144 |
| initial viscosity of water (Pa·s) | 0.001 | cementation factor | 1 |
| initial viscosity of oil (Pa·s) | 0.002 | cementation index | 2 |
| pore compression coefficient (1/Pa) | $6\times10^{-10}$ | saturation index | 2 |
| water compression coefficient (1/Pa) | $5\times10^{-10}$ | temperature (˚C) | 100 |
| oil compression coefficient (1/Pa) | $10\times10^{-10}$ | borehole pressure (Pa) | 17236892.5 |
| initial value of formation saturation | 0.15 | original formation pressure (Pa) | 1378951.4 |
| mud salinity (ppm) | 10000 | Radial mesh number | 100 |

Based on the parameters in Table 1, the invasion depth is selected as $L_1$ = 0.47 m, $L_2$ = 0.59 m, and $L_3$ = 0.71 m to be substituted into equation (8) to obtain the comparison results in Table 2.

**Table 2 Calculated permeability values corresponding to different invasion depths**

| invasion depth (m) | 0.470 | 0.590 | 0.710 |
|---|---|---|---|
| calculated permeability (mD) | 0.645 | 1.034 | 1.512 |

As shown in Table 2, the larger the discriminant value of the invasion depth is, the larger the calculated permeability will be. Therefore, it can be seen that the more accurate the invasion depth obtained by inversion, the closer the obtained permeability to the real formation permeability.

In addition, there is a relatively large error between the calculated permeability ($k$ = 1.5118 mD) using the maximum invasion depth of 0.71 m and the preset formation permeability ($k$ = 1 mD). To solve this problem, α, the volume impact factor, is introduced. Therefore, equation (8) is transformed into

$$k = \frac{\left(L^2 - r_w^2\right)\alpha^2\phi\left(1 - S_{or}\right)\mu_w \ln\left(\frac{r_e}{r_w}\right)}{2T'\left(P_w - P_e\right)}. \quad (9)$$

When $\alpha$ is introduced into equation (9), the calculated permeability is 1.0923 mD ($\alpha$ is 0.85), which is much closer to the preset formation permeability. Thus, in the actual reservoir permeability assessment, it is necessary to introduce a volume impact factor according to the specific reservoir situation to reduce the error. The value of the volume impact factor can be obtained as follows: getting the maximum invasion depth by inversion of array induction logging, inverting the permeability according to the basic parameters in Table 1 and the invasion depth, and obtaining the factor by the ratio of the inversion permeability to the preset formation permeability.

The application area of this model is the southern part of Ordos Basin. This area has entered the development stage, and understanding of the formation has been relatively mature. The formation pressure coefficient in this area is stable; there is basically no abnormal-pressure area. As the main target layer, the mud density of chang 8 of the Yanchang formation is basically fixed when drilling, and the range of variation is very small. Therefore, the volume impact factor α of chang 8 in this area can be the same. However, it needs to be recalculated when the model is used in other layers or areas.

## Invasion time

The basic parameters are set as shown in Table 1. Four different invasion times (24, 36, 48, and 60 h) are set to calculate the relationship between the water saturation and formation resistivity curves at different times to the distance to the borehole axis.

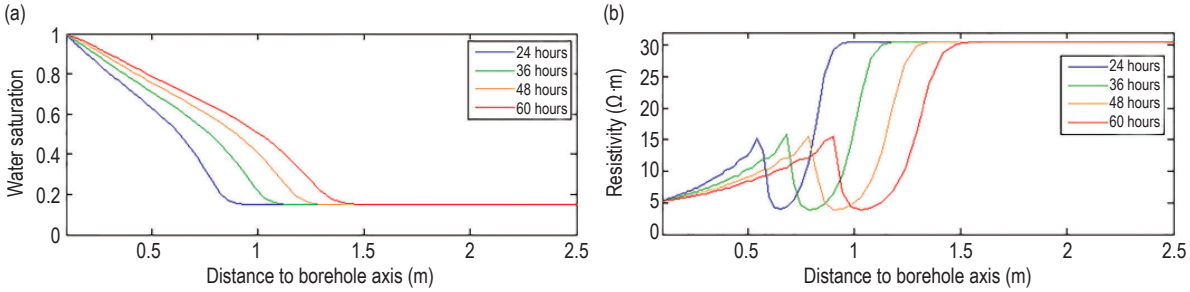


**Figure 2. Water saturation and formation resistivity curves at different invasion times. (a) Water saturation at different invasion times. (b) Formation resistivity at different invasion times.**

According to Figure 2, the invasion depths at the four different invasion times can be obtained, and the predicted permeability values at the four different invasion times can be obtained by substituting the invasion depths into equation (9). The results are shown in Table 3.

**Table 3 Invasion depths and predicted permeability values at different invasion times**

| invasion time (h) | 24 | 36 | 48 | 60 |
|---|---|---|---|---|
| invasion depth (m) | 0.801 | 0.988 | 1.157 | 1.310 |
| predicted permeability (mD) | 0.966 | 0.986 | 1.017 | 1.044 |

As shown in Figure 2 and Table 3, with the increase of the invasion time, the invasion depth increases correspondingly, and the predicted permeability is closer to the real formation permeability. If the invasion depth is shorter than the actual invasion leading edge, with the increase of the invasion depth, the error caused by the

increase of the invasion depth relative to the proportion of the increased invasion depth will be reduced, so it will be closer to the real value. Therefore, when using this model to calculate permeability, the assessment should be made at a late period of invasion to reduce errors.

## Formation porosity

The basic parameters are set as shown in Table 1. Four different porosities (0.05, 0.10, 0.15, and 0.20) are set to calculate the relationship between the water saturation and formation resistivity curves at different porosities to the distance to the borehole axis.

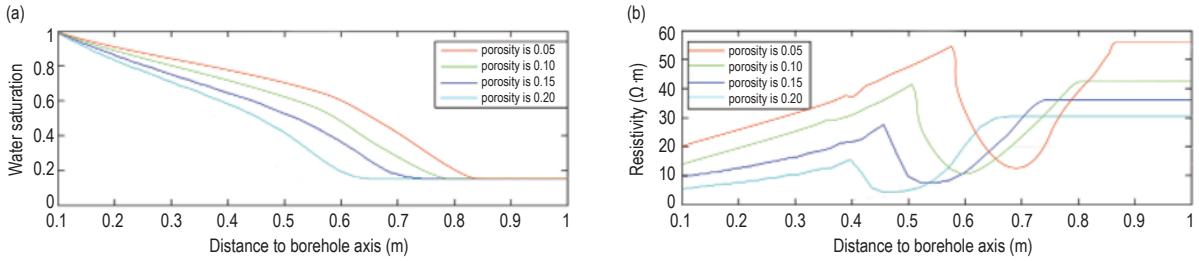


**Figure 3. Water saturation and formation resistivity curves at different porosities. (a) Water saturation at different porosities. (b) Formation resistivity at diffcrent porosities.**

According to Figure 3, the invasion depths at different porosities can be obtained, and the predicted permeability values at different porosities can be obtained by substituting the invasion depths into equation (9). The results are shown in Table 4.

**Table 4 Invasion depths and predicted permeability values at different porosities**

| porosity | 0.05 | 0.10 | 0.15 | 0.20 |
|---|---|---|---|---|
| invasion depth (m) | 0.685 | 0.590 | 0.535 | 0.495 |
| predicted permeability (mD) | 0.998 | 1.025 | 1.054 | 1.107 |

As shown in Figure 3 and Table 4, with the increase of the porosity, the invasion depth decreases, and the permeability increases. The reason is that, with the increase of the porosity, the capillary pressure of formation pores will decrease, leading to an increase in permeability despite an increase in invasion depth. Furthermore, after the porosity is greater than 15%, the permeability growth rate caused by the same porosity increment increases.

## Formation water saturation

The basic parameters are set as shown in Table 1. Three different formation water saturations (0.15, 0.20, and 0.25) are set to calculate the relationship between the water saturation and formation resistivity curves to the distance to the borehole axis.

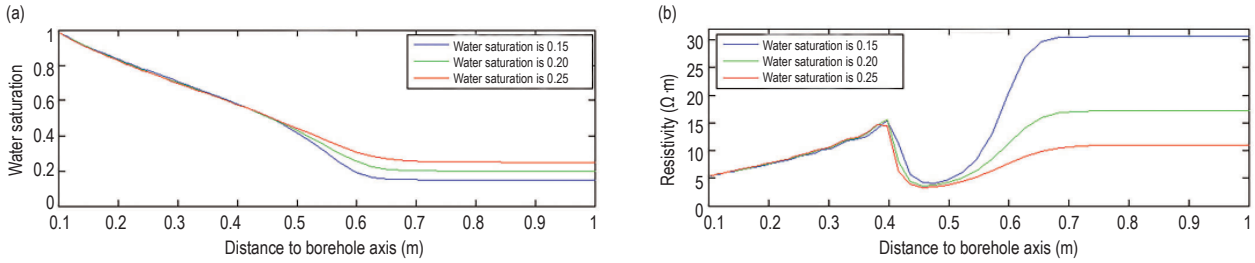


**Figure 4. Water saturation and formation resistivity curves at different water saturations. (a) Invasion depth at different water saturations. (b) Formation resistivity at different water saturations**

According to Figure 4, the invasion depths at different formation water saturations can be obtained, and the predicted permeability values can be obtained by substituting the invasion depths into equation (9). The results are shown in Table 5.

**Table 5 Invasion depths and predicted permeability values at different formation water saturations**

| formation water saturation | 0.15 | 0.20 | 0.25 |
|---|---|---|---|
| invasion depth (m) | 0.590 | 0.599 | 0.601 |
| predicted permeability (mD) | 1.034 | 1.067 | 1.074 |

As shown in Figure 4 and Table 5, with the increase of the formation water saturation, the invasion depth decreases slightly, the predicted permeability also increases slightly, and the overall change is not significant. This is because the variation range of water viscosity in the south of the Ordos Basin is small, so the increase in water saturation has a limited influence on permeability.

## Water viscosity

The basic parameters are set as shown in Table 1. Three different water viscosities ($0.5 \times 10^{-3}$, $1 \times 10^{-3}$, and $1.5 \times 10^{-3}$ Pa·s) are set to calculate the relationship between the water saturation and formation resistivity curves to the distance to the borehole axis.

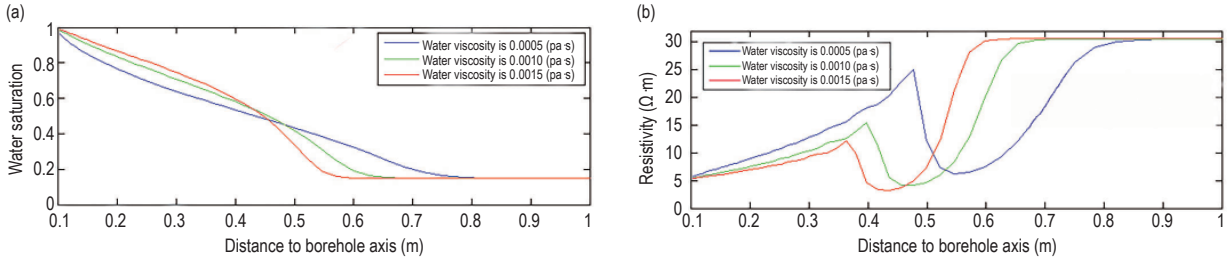


**Figure 5. Water saturation and formation resistivity curves at different water viscosities.**
**(a) Water saturation at different water viscosities. (b) Formation resistivity at different water viscosities.**

According to Figure 5, the invasion depths at different water viscosities can be obtained, and the predicted permeability values can be obtained by substituting the invasion depths into equation (9). The results are shown in Table 6.

**Table 6 Invasion depths and predicted permeability values at different water viscosities**

| water viscosity (Pa·s) | 0.0005 | 0.001 | 0.0015 |
|---|---|---|---|
| invasion depth (m) | 0.715 | 0.590 | 0.540 |
| predicted permeability (mD) | 0.767 | 1.034 | 1.292 |

As shown in Figure 5 and Table 6, with the increase of the water viscosity, the invasion depth decreases gradually, but the predicted permeability is closer to the undisturbed formation permeability. This is because when the water viscosity increases, the viscosities of oil and water become closer, which makes the transitional zone tend to flatten out and become closer to the cylinder. This is close to the premise of the established permeability prediction model.

In addition, there are other factors that influence permeability calculation using mud invasion depth, such as drilling fluid system and logging time. As the research area has been in the development stage, understanding the formation properties is relatively mature. The drilling fluid is stable and basically water-based mud. The drilling fluid density of chang 8 is generally 1.05 g/cm$^3$, and the formation pressure coefficient in this area is stable; thus, the difference between hydrostatic pressure and formation pressure in the same layer is small. At the same time, it generally requires the logging operation to be carried out only after stopping drilling for more than 24 h. After 24 h, the invasion depth can basically reach the maximum invasion depth in this area. Therefore, the types of drilling fluid, the properties of drilling fluid, and logging time in the study area are not discussed in this paper.

# Case study

The above method is applied to process the target

layer in the study area (reservoir boundary pressure is calculated using density curve and formation depth; wellbore pressure is calculated using drilling fluid density and formation depth; and according to the variation range of the maximum invasion depth of the target layer in the study area, the distance between the boundary and the wellbore is set as 3.5 m) and then compare the predicted permeability to the core test permeability. In the comparative analysis figure of permeability, the first trace contains depth; the second trace contains natural gamma ray, spontaneous potential, and two borehole diameter curves; the third trace contains array induction resistivity curves with different detection depths; the fourth trace contains resistivity curves of the flushed zone, the transitional zone, and the undisturbed formation; the fifth trace contains permeability curves before and after inversion and core test permeability; the sixth trace contains the lithology profile; the seventh trace contains interpretation results; the eighth trace contains the invasion profile. As shown in Figure 6, the comparison result between the predicted permeability and core test permeability is well.

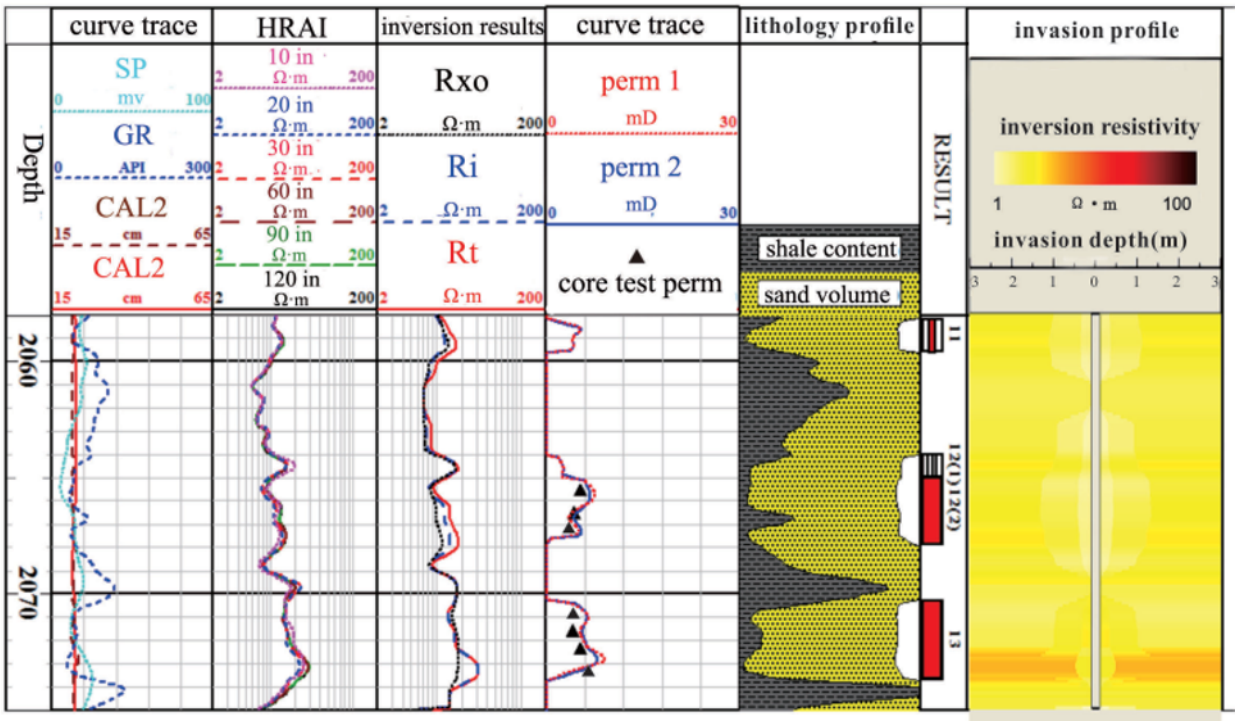


**Figure 6. Comparison between the predicted permeability and core test permeability at 2058~2075 m in well ××.**

As shown in Figure 6, the oil layer is resistant to decreased invasion. There is some difference between the permeability values calculated by the interpretation model and the conventional logging data. The permeability calculated by the model (solid blue line) matches well the core test permeability (black triangle).

**Table 7 Comparison between the predicted permeability and core test permeability**

| Depth (m) | Predicted permeability (mD) | Core test permeability (mD) | Interpretation result |
|---|---|---|---|
| 2065.13 | 4.77 | 4.39 | Oil layer |
| 2066.33 | 4.64 | 4.35 | Oil layer |
| 2067.36 | 4.73 | 4.20 | Oil layer |
| 2070.88 | 5.08 | 4.23 | Oil layer |
| 2071.57 | 5.05 | 4.28 | Oil layer |
| 2072.33 | 5.63 | 5.39 | Oil layer |
| 2073.25 | 5.18 | 5.26 | Oil layer |

Table 7 shows the comparison of the permeability calculated by the permeability model with the core test permeability at 2058~2075 m in well ××. In general, the inversion permeability is slightly greater than the test permeability, and in some depth points, the inversion permeability is less than the test permeability. The average relative error is about 8.9% and is small, which can effectively improve the accuracy of the permeability calculation.

Figure 7 shows the comparison of the permeability calculated by the permeability model for the data of wells in several blocks in the south of Ordos Basin with the core test permeability. As shown in the figure, the sample points are basically distributed near the 45° oblique line. The average absolute error is about 7.4%, and the average relative error is about 8.1%, with both less than one order of magnitude, which indicates that the permeability calculated by the model is accurate and reliable.

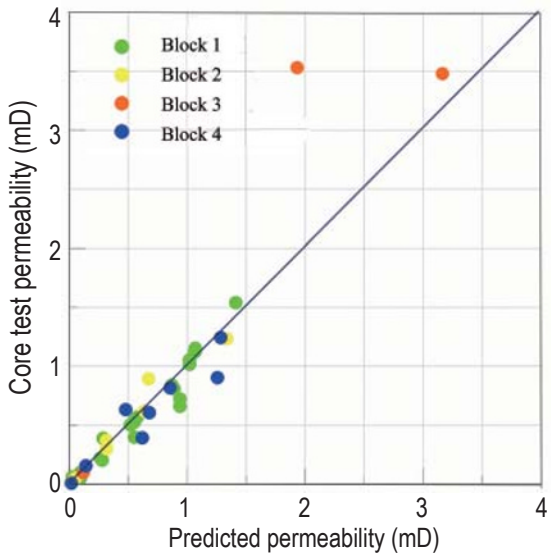


**Figure 7. Comparison of the predicted permeability with the core test permeability.**

## Conclusions

In this paper, a permeability prediction model based on mud invasion depth is established by improving Darcy flow equation. The mud invasion depth obtained by inversion of array induction logging with five parameters is closer to the real formation situation. Therefore, the permeability prediction model based on mud invasion depth can reduce the influence of various complex factors on permeability to a certain extent.

The influencing factors of the established prediction model of permeability are analyzed by means of numerical simulation. The analysis results are as follows.

(1) The longer the mud invasion time, the closer the predicted permeability to the real formation permeability.

(2) With the increase of porosity, the invasion depth decreases, and the predicted permeability increases. Furthermore, after the porosity is greater than 0.15, the permeability growth rate caused by the same porosity increment increases.

(3) There is limited influence on permeability with the increase of formation water saturation.

(4) With the increase of water viscosity, the invasion depth decreases gradually; however, the predicted permeability increases, much closer to the undisturbed formation permeability.

The permeability model is verified by actual well data, and the results show that the permeability calculated by the model is in good accord with the core test permeability. Moreover, the error analysis shows that the average error between the calculated permeability and the core test permeability is less than one order of magnitude. The results verify the reliability of this permeability model.

The permeability model proposed in this paper uses the mud invasion depth inverted by array induction logging with five parameters, but due to the limitation of the lateral detection depth of logging methods, it is still possible to not get the true mud invasion depth of the formation. In this case, the permeability calculated by this model is not accurate enough.

In addition, the permeability model is established in tight sandstone of oil wells, and its applicability in other formation conditions needs to be further verified.

## Acknowledgments

We would like to thank Petroleum Engineering Limited Company of SINOPEC, a well logging company in North China, for providing the logging data and express our gratitude to the reviewers: Wu Hongliang and Hu Song for their valuable comments and the editorial staff for their extensive guidance and assistance with this paper.

## References


Abdulraheem, A., Sabakhy, E., and Ahmed, M., et al., 2007, Estimation of permeability from wireline logs in a middle eastern carbonate reservoir using fuzzy logic: SPE middle east oil and gas show and conference, Bahrain.

Al-Anazi, A. and Gates, I., 2012, Support vector regression to predict porosity and permeability: effect of sample size: Computers & Geosciences, **39**(3), 64–76.

Alfi, M., Hosseini, S. A., Enriquez, D., et al., 2019, A new technique for permeability calculation of core samples from unconventional gas reservoirs: Fuel, **235**(JAN.1), 301–305.

Al-Marzouqi, H., 2018, Digital rock physics: using CT scans to compute rock properties: IEEE Signal Processing Magazine, **35**(2), 121–131.

Chen, Z. Q., Wu, S. Y., BAIai, R., et al., 2017, Logging evaluation for permeability of tight sandstone gas reservoirs based on flow unit classification: a case from Xujiahe Formation in Guang'an area,central Sichuan Basin: Lithologic Reservoirs, **29**(6), 76–83.

Costa, A., 2006, Permeability-porosity relationship: a re-examination of the Kozeny-Carman equation based on a fractal pore-space geometry assumption: Geophysical Research Letters, **33**(2), 87–94.

Darcy, H., 1856, Les Fontaines Publiques de la Ville de Dijon. Dalmont, Paris.

Fan, Y. R., Liu, J. Y., and Ge, X. M., 2018, Permeability evaluation of tight sandstone based on dual T2 cutoff values measured by NMR: Chinese Journal of Geophysics, **61**(4), 1628–1638.

Feng, J. M., 2019, Study on forward Response of array induction logging based on dynamic mud intrusion: PhD Thesis, Yangtze University, Wuhan.

Feng, Z., Hu, X. Y., Meng, Q. X., et al., 2015, Model and method of permeability evaluation based on mud invasion effects: Applied Geophysics, **12**(4), 482–492.

He, Y. F., Wu, X. D., Han, Z. J., et al., 2007, New prediction method of oil well deliverability of low permeability reservoir: Journal of China University of Petroleum (Edition of Natural Science), **31**(5), 69–73.

Lala, A., 2019, An intelligent model for estimating relative permeability in the abu-sennan oil and gas fields, southwestern Egypt: Pure and Applied Geophysics, **176**(102), 4349–4361.

Larson, R. G., Scriven, L. E., and Davis, H. T., 1981, Percolation theory of two phase flow in porous media: Chemical Engineering Science, **36**(1), 57–73.

Li, H., Fan, Y. R., Hu, Y. Y., et al., 2012, Five-parameter inversion method of array induction logging: Journal of China University of Petroleum (Edition of Natural Science), **36**(6), 47–52.

Li, X. L., Lu, Y. L., and Qi, Y., 2015, Permeability evaluation of complex lithology reservoir using ECS log data, Well Logging Technology, **29**(6): 43–45.

Mahdaviara, M., Rostami, A., and Shahbazi, K., 2020, State-of-the-art modeling permeability of the heterogeneous carbonate oil reservoirs using robust computational approaches: Fuel, **268**(1), 117–389.

Mao, Z. Q., Xiao, L., Wang, Z. N., et al., 2013, Estimation of permeability by integrating nuclear magnetic resonance (NMR) logs with mercury injection capillary pressure (MICP) data in tight gas sands: Applied Magnetic Resonance, **44**(4), 449–468.

Mohaghegh, S., 2000, Virtual-intelligence applications in petroleum engineering: part 1-artifical neural networks: Journal of Petroleum Technology, **52**(9), 64–72.

Orlov, D., Ebadi, M., and Muravleva, E., et al., 2021, Different methods of permeability calculation in digital twins of tight sandstones: Journal of Natural Gas Science and Engineering, 103750.

Pape, H., Clauser, C., and Iffland, J.P., 1999, Permeability prediction based on fractal pore-space geometry: Geophysics, **64**(5), 1447–1460.

Pardo, D., and Torres-Verdin, C., 2015, Fast 1D inversion of logging-while-drilling resistivity measurements for improved estimation of formation in high-angle and horizontal wells: Geophysics, **80**(2), E111–E124.

Paulina, I. K., and Edyta, P., 2015, Tight reservoir properties derived by nuclear magnetic resonance, mercury porosimetry and computed microtomography laboratory techniques. case study of palaeozoic clastic rocks: Acta Geophysica, **3**(3), 102–110.

Saemi, M., Ahmadi, M., Varjani, A. Y., et al., 2007, Design of neural networks using genetic algorithm for the permeability estimation of the reservoir: Journal of Petroleum Science & Engineering, **59**(1-2), 97–105.

Singh, N. P., 2019, Permeability prediction from wireline logging and core data: a case study from Assam-Arakan basin: Journal of Petroleum Exploration and Production Technology, **9**(1), 297–305.

Timur, A., 1969, Producible porosity and permeability of sandstone investigated through nuclear magnetic

resonance principle: The Log Analyst, **X**(1), 3–11.

Tong, K. J., Shan, Y. M., Wang, D. C., et al., 2008, CP-curve-based model for estimating reservoir permeability: an example from a sandstone of the Upper Devonian in Tarim Basin: Oil & Gas Geology, **29**(6), 812–818.

Uspenskaya, L. A., Kalmykov, G. A., and Belomestnykh, A. A., 2012, Evaluation of formation permeability from borehole stoneley wave with lithological composition: Moscow University Geology Bulletin, **67**(3), 202–207.

Wang, Q., Tan, M. J., Shi, Y. J., et al., 2020, Prediction of relative permeability and calculation of water cut of tight sandstone reservoir based on radial basis function neural network: Oil Geophysical Prospecting, **55**(4), 864–872.

Zhang, Y., Zeng, J., Cai, J., et al., 2019, A mathematical model for determining oil migration characteristics in low-permeability porous media based on fractal theory: Transport in Porous Media, **129**(3), 633–652.

**Liu Wen-Hui**, a senior engineer, received his Master's degree from the Geophysics and Oil Resource Institute of Yangtze University in 2009, and his Ph.D. degree from the Institute of Geophysics and Geomatics of China University of Geosciences (Wuhan) in 2016. Since 2016, he has worked in the College of Geosciences and Engineering of North China University of Water Resources and Electric Power. His main research interests include geophysical logging and engineering geophysical prospecting.

Contact information:

Email: liuwenhui@ncwu.edu.cn